Electronic Supplementary Information (ESI)

Homoleptic Cyclometalated Dibenzothiophene-NHC-Iridium(III) Complexes for Efficient Blue Phosphorescent Organic Light-Emitting Diodes

Bo-Sun Yun, So-Yoen Kim, Jin-Hyoung Kim, Ho-Jin Son* and Sang Ook Kang*

Department of Advanced Materials Chemistry, Korea University, Sejong 30019, South Korea,

General Information

Spectroscopic Measurements. The steady-state absorption spectra were measured using a UV-Vis-NIR spectrophotometer (Agilent Technologies, Cary 5000). The steady-state emission spectra were measured using a fluorescence spectrophotometer (Varian, Cary Eclipse) equipped with high-performance R928 photomultiplier detector (high-performance R928) and CW Xenon lamp. For the measurement of phosphorescence spectrum at 77 K, the third harmonic (355 nm) pulse of a Q-switched Nd:YAG laser (Continuum, Surelite II; pulse width of 4.5 ns) was used as an excitation source.[1] The phosphorescence spectra were recorded using an ICCD detector (Andor, iStar) equipped with a monochromator (DongWoo Optron, Monora 500i). The temporal profiles were measured using a photomultiplier (Zolix Instruments Co., CR 131) and a digital oscilloscope (Tektronix, TDS-784D). Oxygen in the sample solutions was removed through the argon purging method.

Quantum Yield. Absolute PLQYs were obtained using a Quantaurus-QY measurement system (C11347-11, Hamamatsu Photonics), and all the samples were excited at 355 nm.

Electrochemical Analysis. The cyclic voltammetry experiments were performed using an electrochemical analyzer (Bioanalytical System Inc., BAS 100). The three-electrode cell system is comprised of a platinum disk (diameter = 1.6 mm) electrode as the working electrode, and platinum wire and $Ag/AgNO_3$ as a counter, and reference electrodes, respectively. Distilled and argon purged DMF was used as the solvent with 1 mM tetrabutylammonium perchlorate electrolyte as the supporting electrolyte. The potential values were calibrated concerning the Fc/Fc^+ (Fc = Ferrocene) redox couple.

Theoretical Calculation. All the calculations were performed using the *Gaussian 09* program package.[2] The ground-state geometry was fully optimized using the density functional theory (DFT) level of the B3LYP (UB3LTYP for triplet calculation) method.[3,4] The 6-31G(d,p) and LANL2DZ basis sets were applied for non-metal atoms and iridium, respectively. The isodensity plots (contour = 0.03 a.u.) of the frontier orbitals were visualized by the GaussView 6 program. The TD-DFT calculation was performed to evaluate the vertical transition energies and oscillator strength for the singlet and triplet transitions.

X-ray Crystallography. The X-ray diffraction data collection were recorded by a Bruker APEX3 CCD detector system single-crystal X-ray diffractometer equipped with a sealed-tube X-ray source (50 kV × 30 mA) using graphite monochromatic Mo Kα radiation (λ = 0.71073 Å). The unit cell constants were determined using a set of 45 narrow-frame (0.3° in ω) scans. The double-pass method of scanning was used to exclude noise. The collected frames were integrated using an orientation matrix determined from the narrow-frame scans. The SMART software package was used for data collection, and SAINT was used for frame integration.[5] The final cell constants were determined through the global refinement of the *xyz* centroids of the reflections harvested from the entire data set. Structure solution and refinement were carried out using the SHELXTL-PLUS software package.[6]

Thermal Analysis. Thermogravimetric analyses of all complexes were recorded on a Perkin-Elmer TGA 4000 instrument in the temperature range of 30 – 800 ℃ under N_2 flow with a heating rate of 10 ℃ min^{-1}.

Device Fabrication and Characterization. The OLED devices were fabricated on glass substrates, which were pre-coated with a 150 nm indium tin oxide (ITO) layer having a sheet resistance of 10 Ω/square. The ITO glass was precleaned sequentially with acetone (30 min), *N*-methyl-2-pyrrolidone (NMP) (30 min), deionized water, and isopropyl alcohol (IPA) (30 min), in an ultrasonic bath. The cleaned ITO glass was used immediately to fabricate the OLEDs. Before usage, the ITO substrates were treated with oxygen plasma. The organic and metal layers were deposited onto the ITO-coated glass substrate by thermal evaporation, and device fabrication was completed in a single cycle, without breaking the vacuum. The coated film was shadow masked to give four identical devices of area (2 mm × 2 mm). All the fabricated devices were encapsulated in N_2 glove box, before taking measurements. The current-voltage characteristics of OLEDs were analyzed using a source measurement unit (Keithley 2635B). The electroluminescence spectra, luminance, and CIE coordinates were measured by a spectroradiometer (Konica Minolta CS-2000). Assuming Lambertian emission, the external quantum efficiency (EQE) was calculated from the luminance, current density, and electroluminescence spectrum.

(a)

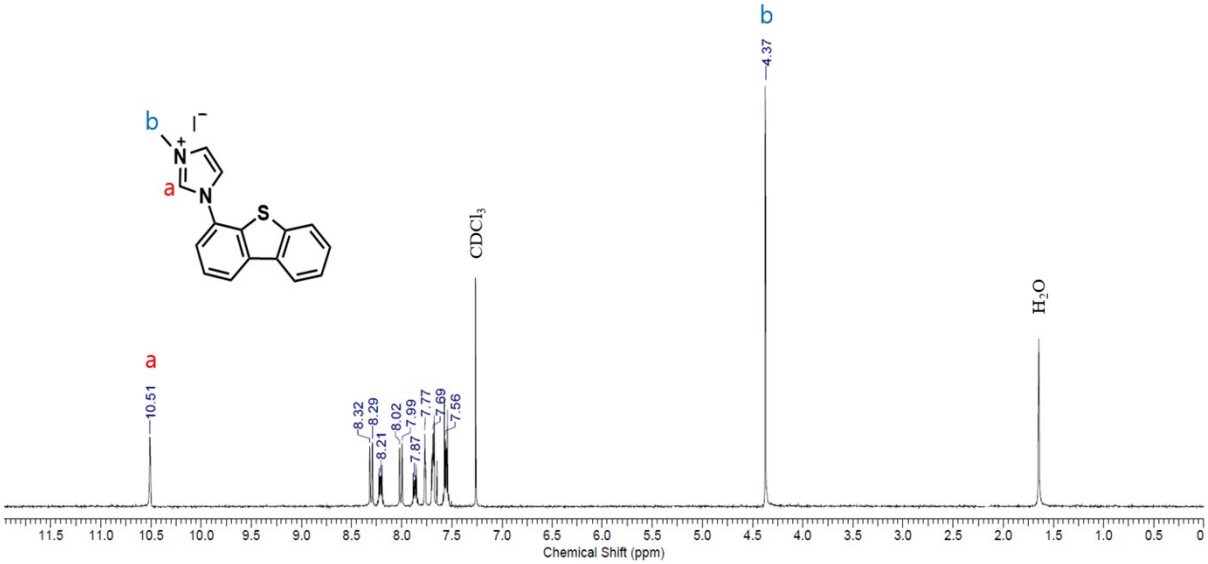

(b)

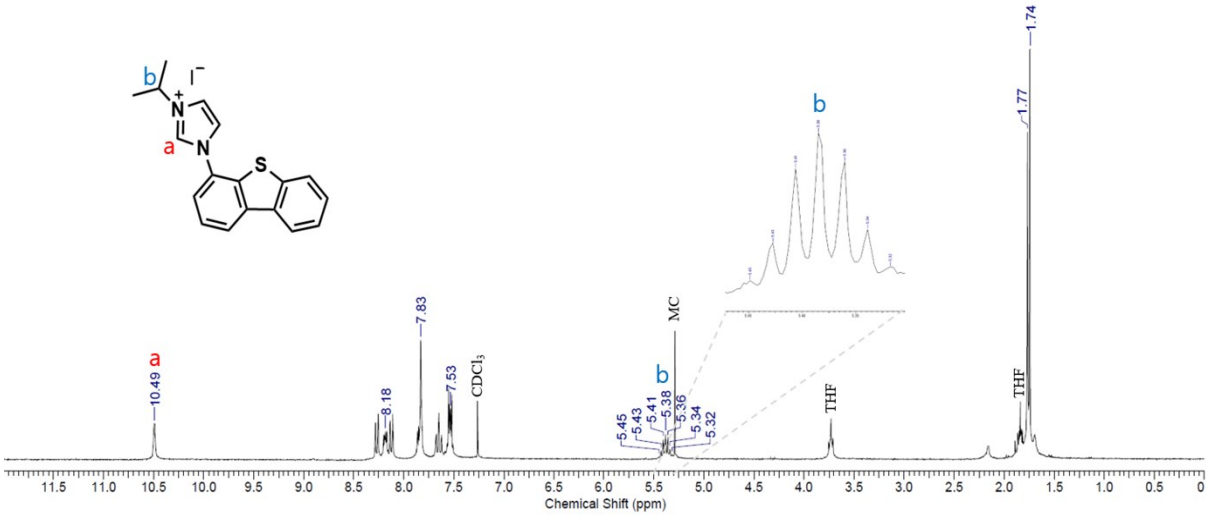

Fig. S1 ^{1}H-NMR spectra of (a) 1-(dibenzo[*b*,*d*]thiophen-4-yl)-3-methyl-1*H*-imidazol-3-ium iodide and (b) 1-(dibenzo[*b*,*d*]thiophen-4-yl)-3-isopropyl-1*H*-imidazol-3-ium iodide.

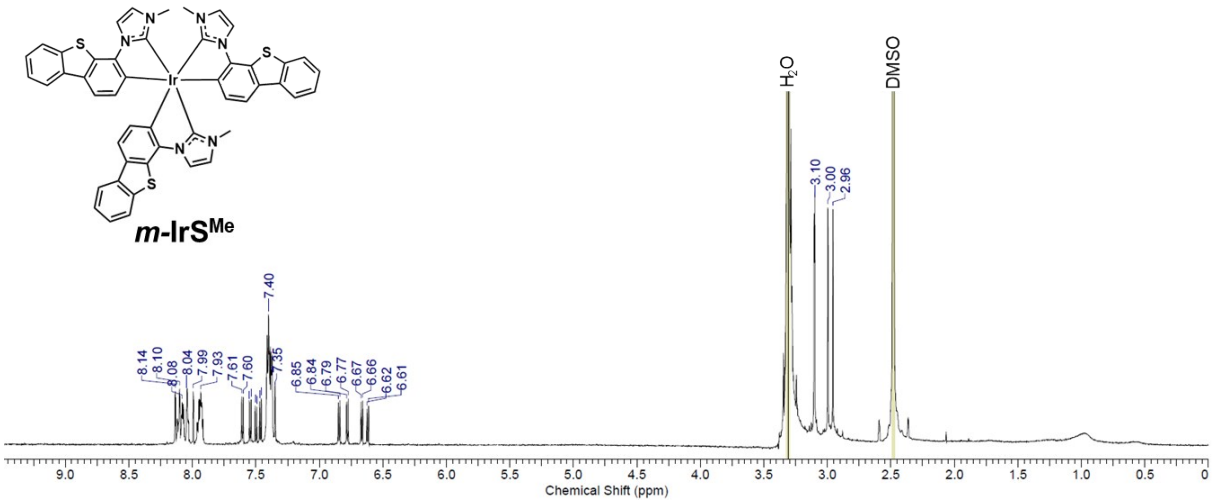

Fig. S2 ^{1}H-NMR spectra of ***m*-IrS^{Me}**.

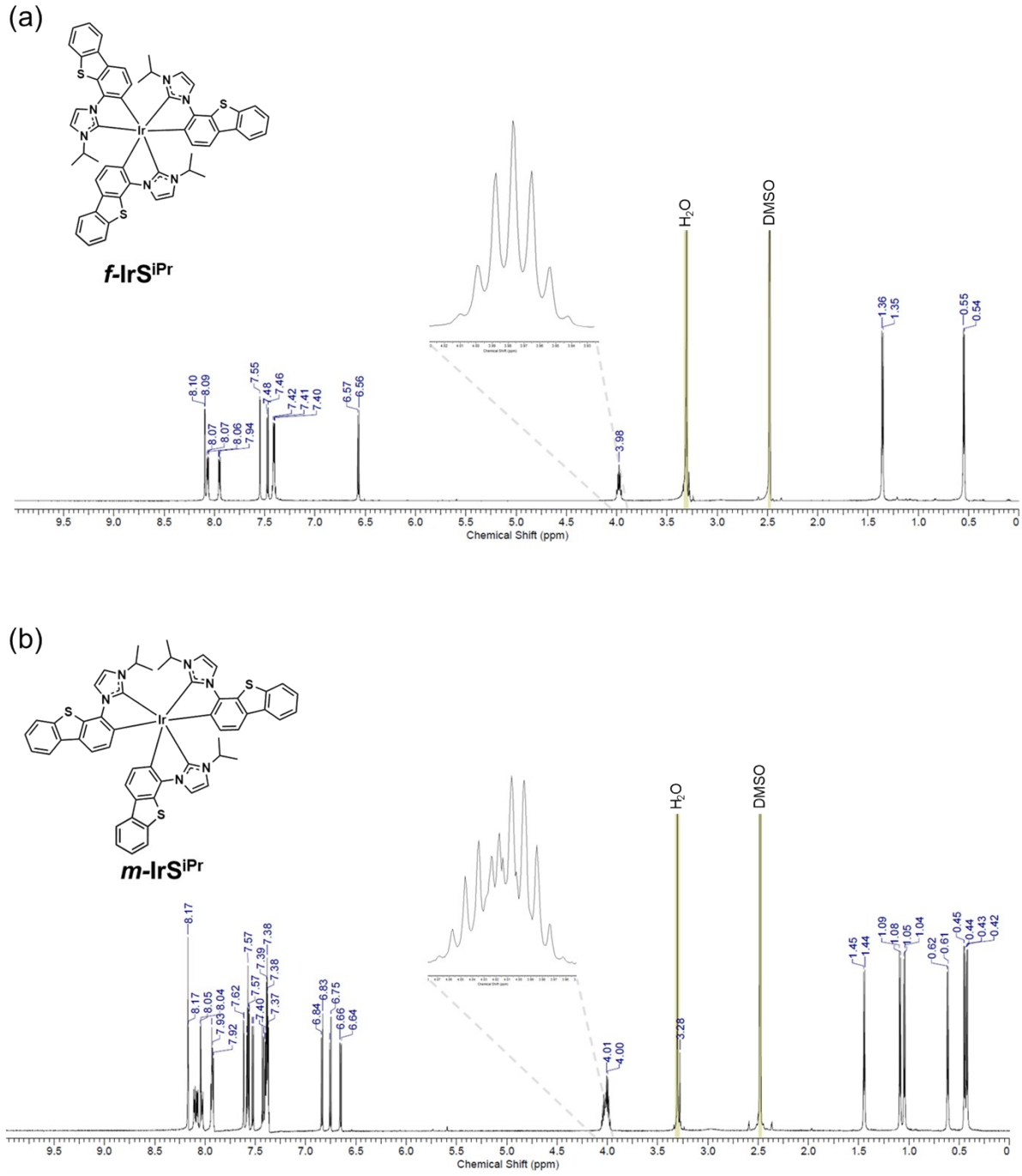

Fig. S3 ^{1}H-NMR spectra of (a) ***f*-IrS^{iPr}** and (b) ***m*-IrS^{iPr}**.

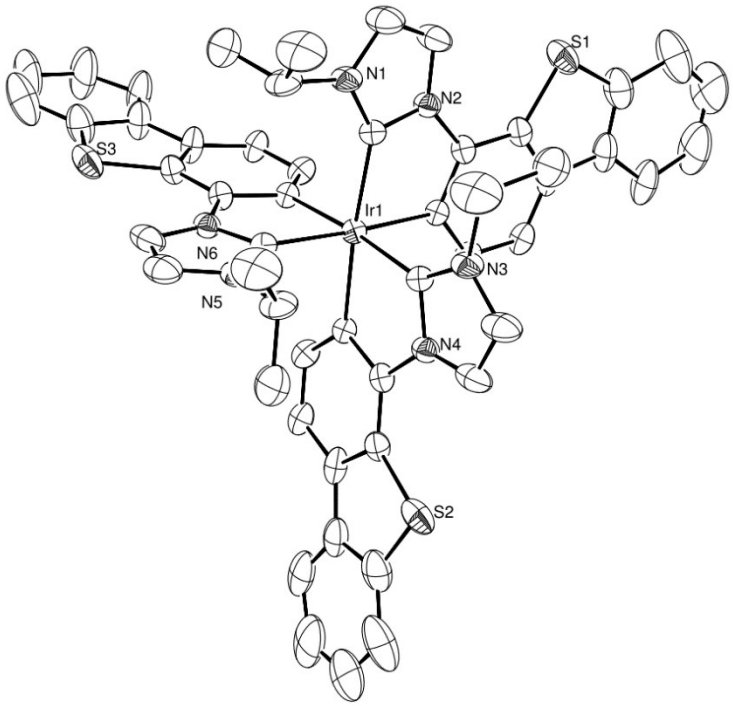

Fig. S4 ORTEP drawing of compound ***f*-IrS^{iPr}** with 30% probability for the thermal ellipsoids. Hydrogens were omitted for clarity.

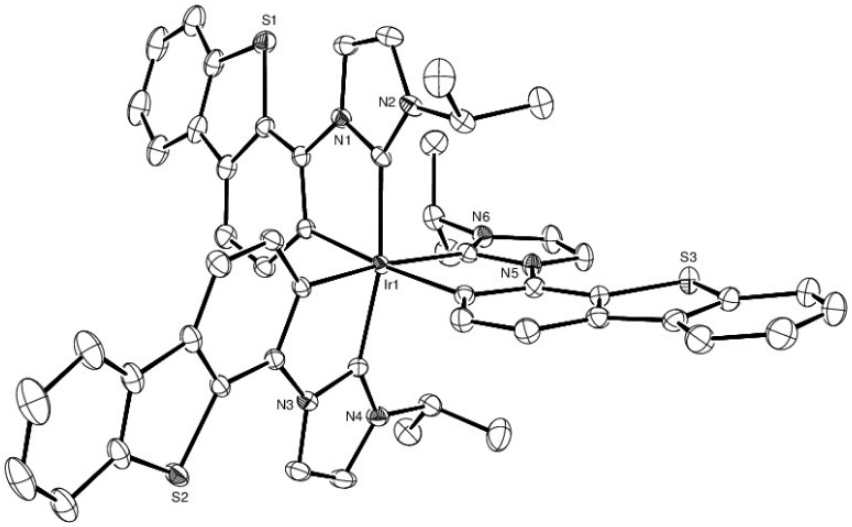

Fig. S5 ORTEP drawing of compound ***m*-IrS^{iPr}** with 30% probability for the thermal ellipsoids. Hydrogens were omitted for clarity.

Table S1 Crystal data and structure refinement for ***f*-IrS^{iPr}** and ***m*-IrS^{iPr}**

	***f*-IrS^{iPr}**	***m*-IrS^{iPr}**
Identification code	CCDC-2048872	CCDC-2048745
Empirical formula	C_{54} H_{45} Ir N_6 S_3	C_{54} H_{45} Ir N_6 S_3
Formula weight	1066.34	1066.36
Temperature	296(2) K	293(2) K
Wavelength	0.71073 Å	0.71073 Å
Crystal system,	Trigonal	Triclinic
Space group	*P*-3	*P*-1
Unit cell dimensions	a = 16.7503(1) Å	a = 10.7871(9) Å, α = 87.345(3)º
	b = 16.7503(1) Å	b = 13.0111(1) Å, β = 83.806(3)º
	c = 10.5649(9) Å, γ = 120.0º	c = 19.3462(2) Å, γ = 71.912(3)º
Volume	2567.1(4) Å^3	2365.8(4) Å^3
Z, D_{calc}	2, 1.380 Mg/cm^3	2, 1.322 Mg/cm^3
F(000)	1072	982
Crystal size	0.40 × 0.10 × 0.12 mm	0.40 × 0.38 × 0.10 mm
θ range for data collection	2.385 to 28.314º	2.118 to 28.364º
Limiting indices	$-22 \le h \le 22$, $-22 \le k \le 22$, $-14 \le l \le 12$	$-14 \le h \le 14$, $-16 \le k \le 17$, $-25 \le l \le 25$
Reflections collected / unique	19853 / 4252 [R(int) = 0.0469]	86000 / 12817 [R(int) = 0.0340]
Completeness to θ = 25.242	99.5%	99.9%
Refinement method	Full-matrix least-squares on F^2	Full-matrix least-squares on F^2
Data / restraints / parameters	4252 / 0 / 195	12817 / 0 / 577
Goodness-of-fit on F^2	1.046	0.648
Final R indices [I > 2θ (I)]	$^aR_1$ = 0.0390, ^{b}wR_2 = 0.1057	$^aR_1$ = 0.0196, ^{b}wR_2 = 0.0659
R indices (all data)	$^aR_1$ = 0.0563, ^{b}wR_2 = 0.1234	$^aR_1$ = 0.0233, ^{b}wR_2 = 0.0728
Largest diff. peak and hole	0.787 and −1.007 e.Å^{-3}	1.156 and −0.473 e.Å^{-3}

$^aR_1 = \sum||F_o|-|F_c|| / \sum|F_o|$ (based on reflections with $F_o^2 > 2\sigma F^2$), $^bwR_2 = [\sum[w (F_o^2-F_c^2)^2] / \sum[w (F_o^2)^2]]^{1/2}$; $w = 1/[\sigma^2 (F_o^2) + (0.095P)^2]$; $P = [\max(F_o^2, 0) + 2F_c^2]/3$(also with $F_o^2 > 2\sigma F^2$)

Table S2 Bond lengths [Å] for ***f*-IrS^{iPr}**

Ir(1)-C(13)	2.042(5)	C(3)-C(4)	1.369(9)
Ir(1)-C(1)	2.087(4)	C(4)-C(5)	1.398(8)
S(1)-C(12)	1.739(8)	C(4)-C(7)	1.454(8)
S(1)-C(5)	1.762(6)	C(5)-C(6)	1.395(7)
N(1)-C(13)	1.328(6)	C(7)-C(8)	1.379(1)
N(1)-C(15)	1.391(8)	C(7)-C(12)	1.399(1)
N(1)-C(16)	1.477(8)	C(8)-C(9)	1.422(1)
N(2)-C(14)	1.359(7)	C(9)-C(10)	1.392(2)
N(2)-C(13)	1.393(6)	C(10)-C(11)	1.325(2)
N(2)-C(6)	1.424(6)	C(11)-C(12)	1.417(1)
C(1)-C(6)	1.385(7)	C(14)-C(15)	1.303(9)
C(1)-C(2)	1.414(7)	C(16)-C(18)	1.526(1)
C(2)-C(3)	1.361(7)	C(16)-C(17)	1.545(1)

Symmetry transformations used to generate equivalent atoms: #1 −y, x−y+1, z / #2 −x+y−1, −x, z

Table S3 Angles [°] for ***f*-IrS^{iPr}**

C(13)#1-Ir(1)-C(13)#2	100.0(2)	C(3)-C(4)-C(5)	119.7(5)
C(13)#1-Ir(1)-C(13)	100.0(2)	C(3)-C(4)-C(7)	128.6(6)
C(13)#2-Ir(1)-C(13)	100.0(2)	C(5)-C(4)-C(7)	111.7(6)
C(13)#1-Ir(1)-C(1)	86.4(2)	C(6)-C(5)-C(4)	119.6(5)
C(13)#2-Ir(1)-C(1)	173.6(2)	C(6)-C(5)-S(1)	128.1(5)
C(13)-Ir(1)-C(1)	78.7(2)	C(4)-C(5)-S(1)	112.3(4)
C(13)#1-Ir(1)-C(1)#2	173.6(2)	C(1)-C(6)-C(5)	121.4(5)
C(13)#2-Ir(1)-C(1)#2	78.7(2)	C(1)-C(6)-N(2)	114.2(4)
C(13)-Ir(1)-C(1)#2	86.4(2)	C(5)-C(6)-N(2)	124.4(5)
C(1)-Ir(1)-C(1)#2	94.9(2)	C(8)-C(7)-C(12)	117.9(7)
C(13)#1-Ir(1)-C(1)#1	78.7(2)	C(8)-C(7)-C(4)	129.9(9)
C(13)#2-Ir(1)-C(1)#1	86.4(2)	C(12)-C(7)-C(4)	112.1(6)
C(13)-Ir(1)-C(1)#1	173.6(2)	C(7)-C(8)-C(9)	118.3(1)
C(1)-Ir(1)-C(1)#1	94.9(2)	C(10)-C(9)-C(8)	121.2(1)
C(1)#2-Ir(1)-C(1)#1	94.9(2)	C(11)-C(10)-C(9)	121.9(1)
C(12)-S(1)-C(5)	91.1(4)	C(10)-C(11)-C(12)	117.1(1)
C(13)-N(1)-C(15)	110.3(5)	C(7)-C(12)-C(11)	123.7(9)
C(13)-N(1)-C(16)	123.8(5)	C(7)-C(12)-S(1)	112.7(5)
C(15)-N(1)-C(16)	125.9(5)	C(11)-C(12)-S(1)	123.6(9)
C(14)-N(2)-C(13)	110.2(5)	N(1)-C(13)-N(2)	103.9(4)
C(14)-N(2)-C(6)	133.2(5)	N(1)-C(13)-Ir(1)	140.8(4)
C(13)-N(2)-C(6)	116.7(4)	N(2)-C(13)-Ir(1)	115.1(3)
C(6)-C(1)-C(2)	116.7(4)	C(15)-C(14)-N(2)	107.5(6)
C(6)-C(1)-Ir(1)	115.2(3)	C(14)-C(15)-N(1)	108.1(6)
C(2)-C(1)-Ir(1)	128.2(4)	N(1)-C(16)-C(18)	110.2(6)
C(3)-C(2)-C(1)	122.3(5)	N(1)-C(16)-C(17)	109.5(6)
C(2)-C(3)-C(4)	120.3(5)	C(18)-C(16)-C(17)	113.5(7)

Symmetry transformations used to generate equivalent atoms: #1 −y, x−y+1, z / #2 −x+y−1, −x, z

Table S4 Bond lengths [Å] for ***m*-IrS^{iPr}**

Ir(1)-C(31)	2.026(2)	C(7)-C(8)	1.398(5)
Ir(1)-C(13)	2.044(2)	C(8)-C(9)	1.364(5)
Ir(1)-C(19)	2.066(2)	C(9)-C(10)	1.401(3)
Ir(1)-C(49)	2.067(2)	C(11)-C(12)	1.388(3)
Ir(1)-C(1)	2.089(2)	C(14)-C(15)	1.342(3)
Ir(1)-C(37)	2.099(2)	C(16)-C(17)	1.502(3)
S(1)-C(10)	1.747(3)	C(16)-C(18)	1.517(3)
S(1)-C(11)	1.761(2)	C(19)-C(30)	1.406(3)
S(2)-C(28)	1.753(3)	C(19)-C(20)	1.411(3)
S(2)-C(29)	1.758(2)	C(20)-C(21)	1.382(3)
S(3)-C(46)	1.751(2)	C(21)-C(22)	1.397(3)
S(3)-C(47)	1.754(2)	C(22)-C(29)	1.409(3)
N(1)-C(13)	1.369(3)	C(22)-C(23)	1.452(3)
N(1)-C(15)	1.390(3)	C(23)-C(28)	1.393(4)
N(1)-C(12)	1.424(3)	C(23)-C(24)	1.397(3)
N(2)-C(13)	1.363(3)	C(24)-C(25)	1.387(4)
N(2)-C(14)	1.390(3)	C(25)-C(26)	1.378(5)
N(2)-C(16)	1.474(3)	C(26)-C(27)	1.380(5)
N(3)-C(31)	1.368(3)	C(27)-C(28)	1.394(3)
N(3)-C(33)	1.392(3)	C(29)-C(30)	1.396(3)
N(3)-C(30)	1.417(3)	C(32)-C(33)	1.335(3)
N(4)-C(31)	1.359(3)	C(34)-C(35)	1.508(3)
N(4)-C(32)	1.391(3)	C(34)-C(36)	1.521(4)
N(4)-C(34)	1.471(3)	C(37)-C(48)	1.404(3)
N(5)-C(49)	1.368(3)	C(37)-C(38)	1.415(3)
N(5)-C(51)	1.385(2)	C(38)-C(39)	1.377(3)
N(5)-C(48)	1.424(2)	C(39)-C(40)	1.398(3)
N(6)-C(49)	1.361(2)	C(40)-C(47)	1.413(3)
N(6)-C(50)	1.386(3)	C(40)-C(41)	1.451(3)
N(6)-C(52)	1.468(3)	C(41)-C(46)	1.392(3)
C(1)-C(12)	1.408(3)	C(41)-C(42)	1.402(3)
C(1)-C(2)	1.411(3)	C(42)-C(43)	1.390(4)
C(2)-C(3)	1.386(3)	C(43)-C(44)	1.380(4)
C(3)-C(4)	1.399(3)	C(44)-C(45)	1.374(4)
C(4)-C(11)	1.411(3)	C(45)-C(46)	1.408(3)
C(4)-C(5)	1.452(3)	C(47)-C(48)	1.399(3)
C(5)-C(10)	1.392(4)	C(50)-C(51)	1.334(3)
C(5)-C(6)	1.397(4)	C(52)-C(53)	1.517(3)
C(6)-C(7)	1.389(4)	C(52)-C(54)	1.524(3)

Table S5 Angles [°] for ***m*-IrS^{iPr}**

C(31)-Ir(1)-C(13)	168.3(8)	N(2)-C(16)-C(18)	111.1(2)
C(31)-Ir(1)-C(19)	78.2(8)	C(17)-C(16)-C(18)	111.1(2)
C(13)-Ir(1)-C(19)	94.4(8)	C(30)-C(19)-C(20)	116.1(2)
C(31)-Ir(1)-C(49)	99.7(8)	C(30)-C(19)-Ir(1)	115.4(1)
C(13)-Ir(1)-C(49)	89.3(8)	C(20)-C(19)-Ir(1)	128.4(2)
C(19)-Ir(1)-C(49)	169.3(8)	C(21)-C(20)-C(19)	122.7(2)
C(31)-Ir(1)-C(1)	93.0(8)	C(20)-C(21)-C(22)	120.3(2)
C(13)-Ir(1)-C(1)	77.9(8)	C(21)-C(22)-C(29)	118.7(2)
C(19)-Ir(1)-C(1)	91.6(8)	C(21)-C(22)-C(23)	129.1(2)
C(49)-Ir(1)-C(1)	99.1(8)	C(29)-C(22)-C(23)	112.2(2)
C(31)-Ir(1)-C(37)	90.8(8)	C(28)-C(23)-C(24)	118.8(2)
C(13)-Ir(1)-C(37)	98.7(8)	C(28)-C(23)-C(22)	112.4(2)
C(19)-Ir(1)-C(37)	91.7(8)	C(24)-C(23)-C(22)	128.8(2)
C(49)-Ir(1)-C(37)	77.8(8)	C(25)-C(24)-C(23)	119.1(3)
C(1)-Ir(1)-C(37)	175.4(7)	C(26)-C(25)-C(24)	121.0(3)
C(10)-S(1)-C(11)	91.6(1)	C(25)-C(26)-C(27)	121.5(2)
C(28)-S(2)-C(29)	91.6(1)	C(26)-C(27)-C(28)	117.3(3)
C(46)-S(3)-C(47)	91.1(1)	C(23)-C(28)-C(27)	122.3(3)
C(13)-N(1)-C(15)	111.3(2)	C(23)-C(28)-S(2)	112.3(2)
C(13)-N(1)-C(12)	116.8(2)	C(27)-C(28)-S(2)	125.4(2)
C(15)-N(1)-C(12)	131.7(2)	C(30)-C(29)-C(22)	120.0(2)
C(13)-N(2)-C(14)	110.8(2)	C(30)-C(29)-S(2)	128.4(2)
C(13)-N(2)-C(16)	124.8(2)	C(22)-C(29)-S(2)	111.5(2)
C(14)-N(2)-C(16)	124.3(2)	C(29)-C(30)-C(19)	122.2(2)
C(31)-N(3)-C(33)	110.9(2)	C(29)-C(30)-N(3)	124.5(2)
C(31)-N(3)-C(30)	116.3(2)	C(19)-C(30)-N(3)	113.3(2)
C(33)-N(3)-C(30)	132.8(2)	N(4)-C(31)-N(3)	104.3(2)
C(31)-N(4)-C(32)	110.6(2)	N(4)-C(31)-Ir(1)	139.0(2)
C(31)-N(4)-C(34)	124.3(2)	N(3)-C(31)-Ir(1)	116.7(1)
C(32)-N(4)-C(34)	125.1(2)	C(33)-C(32)-N(4)	107.6(2)
C(49)-N(5)-C(51)	111.1(2)	C(32)-C(33)-N(3)	106.6(2)
C(49)-N(5)-C(48)	117.3(2)	N(4)-C(34)-C(35)	111.7(2)
C(51)-N(5)-C(48)	131.5(2)	N(4)-C(34)-C(36)	110.3(2)
C(49)-N(6)-C(50)	110.4(2)	C(35)-C(34)-C(36)	112.4(2)
C(49)-N(6)-C(52)	125.2(2)	C(48)-C(37)-C(38)	115.7(2)
C(50)-N(6)-C(52)	124.4(2)	C(48)-C(37)-Ir(1)	115.3(2)
C(12)-C(1)-C(2)	115.9(2)	C(38)-C(37)-Ir(1)	128.9(2)
C(12)-C(1)-Ir(1)	115.1(1)	C(39)-C(38)-C(37)	123.0(2)

C(2)-C(1)-Ir(1)	129.0(2)	C(38)-C(39)-C(40)	120.2(2)
C(3)-C(2)-C(1)	122.4(2)	C(39)-C(40)-C(47)	119.0(2)
C(2)-C(3)-C(4)	120.5(2)	C(39)-C(40)-C(41)	129.0(2)
C(3)-C(4)-C(11)	118.4(2)	C(47)-C(40)-C(41)	112.0(2)
C(3)-C(4)-C(5)	129.5(2)	C(46)-C(41)-C(42)	119.1(2)
C(11)-C(4)-C(5)	112.0(2)	C(46)-C(41)-C(40)	112.0(2)
C(10)-C(5)-C(6)	118.8(2)	C(42)-C(41)-C(40)	128.8(2)
C(10)-C(5)-C(4)	112.5(2)	C(43)-C(42)-C(41)	119.0(3)
C(6)-C(5)-C(4)	128.7(3)	C(44)-C(43)-C(42)	120.9(3)
C(7)-C(6)-C(5)	119.4(3)	C(45)-C(44)-C(43)	121.6(2)
C(6)-C(7)-C(8)	120.4(3)	C(44)-C(45)-C(46)	117.8(3)
C(9)-C(8)-C(7)	121.0(3)	C(41)-C(46)-C(45)	121.5(2)
C(8)-C(9)-C(10)	118.4(3)	C(41)-C(46)-S(3)	112.9(2)
C(5)-C(10)-C(9)	121.9(3)	C(45)-C(46)-S(3)	125.5(2)
C(5)-C(10)-S(1)	112.4(2)	C(48)-C(47)-C(40)	119.4(2)
C(9)-C(10)-S(1)	125.8(2)	C(48)-C(47)-S(3)	128.6(2)
C(12)-C(11)-C(4)	120.0(2)	C(40)-C(47)-S(3)	111.9(2)
C(12)-C(11)-S(1)	128.4(2)	C(47)-C(48)-C(37)	122.7(2)
C(4)-C(11)-S(1)	111.5(2)	C(47)-C(48)-N(5)	123.6(2)
C(11)-C(12)-C(1)	122.5(2)	C(37)-C(48)-N(5)	113.6(2)
C(11)-C(12)-N(1)	124.2(2)	N(6)-C(49)-N(5)	104.2(2)
C(1)-C(12)-N(1)	113.2(2)	N(6)-C(49)-Ir(1)	140.0(2)
N(2)-C(13)-N(1)	104.0(2)	N(5)-C(49)-Ir(1)	115.8(1)
N(2)-C(13)-Ir(1)	139.7(2)	C(51)-C(50)-N(6)	108.0(2)
N(1)-C(13)-Ir(1)	116.3(1)	C(50)-C(51)-N(5)	106.4(2)
C(15)-C(14)-N(2)	107.5(2)	N(6)-C(52)-C(53)	109.7(2)
C(14)-C(15)-N(1)	106.4(2)	N(6)-C(52)-C(54)	110.6(2)
N(2)-C(16)-C(17)	110.8(2)	C(53)-C(52)-C(54)	111.8(2)

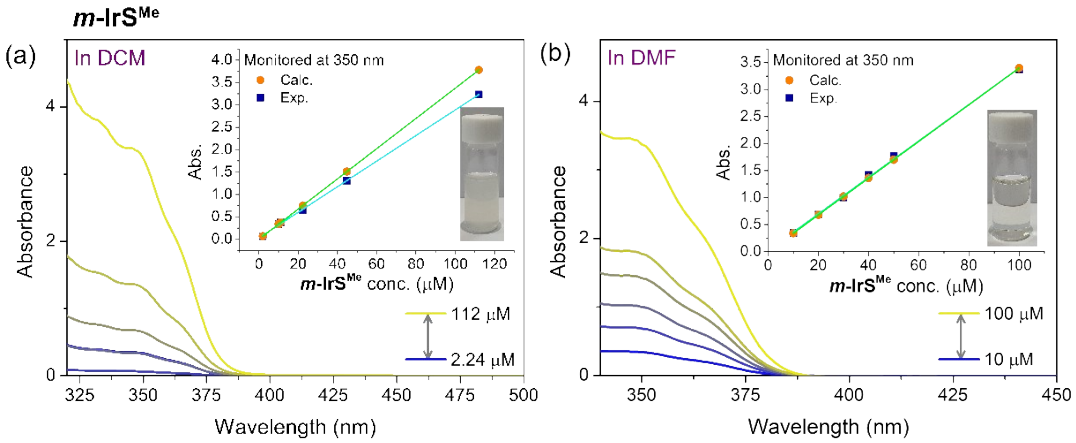

Fig. S6. Absorbance changes versus concentration variation of ***m*-IrS^{Me}** in dichloromethane (DCM, a) and dimethylformamide (DMF, b). Inset graphs show the linear relationship between concentration and absorbance of ***m*-IrS^{Me}** monitored at 350 nm. The linear green lines show the behavior expected in the absence of aggregation between dissolved Ir(III) complexes.

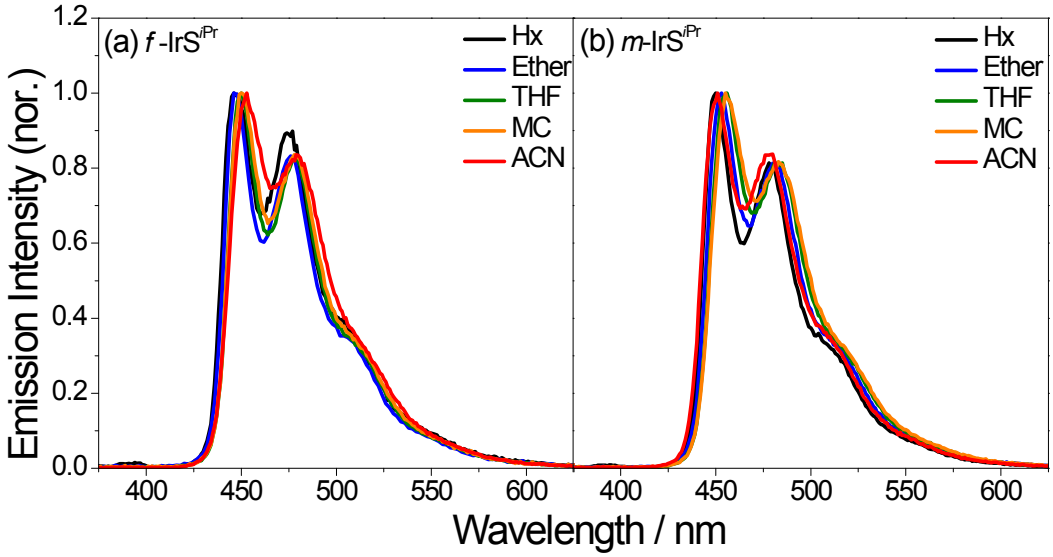

Fig. S7 Emission spectra of (a) ***f*-IrS^{iPr}** and (b) ***m*-IrS^{iPr}** in different solvents.

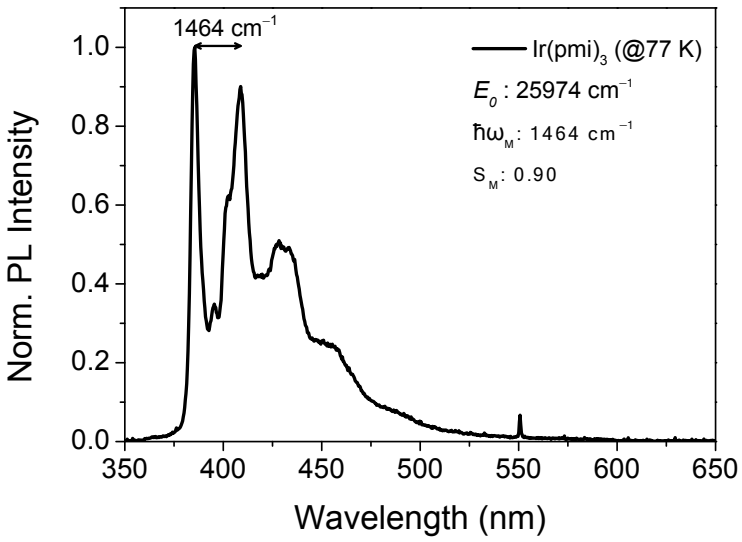

Fig. S8 Phosphorescence spectrum of Ir(pmi)$_3$ complexes at 77 K.

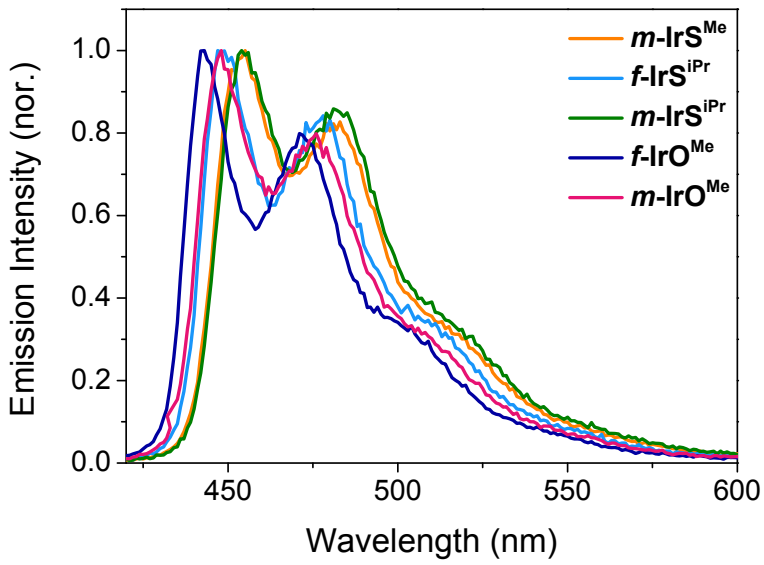

Fig. S9 Emission spectra of iridium complexes 10 wt.% in PMMA film.

Table S6 Electrochemical properties of Ir(III) complexes in DMF solution.

	E_{onset}^{ox} [V]	E_g [V][a]	IP [eV][b]	EA [eV][c]
***m*-IrS^{Me}**	0.11	3.27	− 4.91	− 1.70
***f*-IrS^{iPr}**	0.17	3.32	− 4.97	− 1.74
***m*-IrS^{iPr}**	0.14	3.26	− 4.94	− 1.72
***f*-IrO^{Me}**	0.13	3.37	− 4.93	− 1.66
***m*-IrO^{Me}**	0.06	3.28	− 4.86	− 1.66

[a] E_g is taken as the energy corresponding to the 10% intensity of the lowest energy absorption band edge. [b] The ionization potential (IP) energies are calculated from the oxidation potential, IP (eV) = $-e(E_{onset}^{ox} + 4.8)$, where E_{onset}^{ox} are electrochemical potential over ferrocenium/ferrocene reference (vs Ag/AgCl), and 4.8 eV is the value of Fc with respect to zero vacuum level. [c] The electron affinity (EA) levels are calculated according to the following equations: EA (eV) = e(IP – E_g).

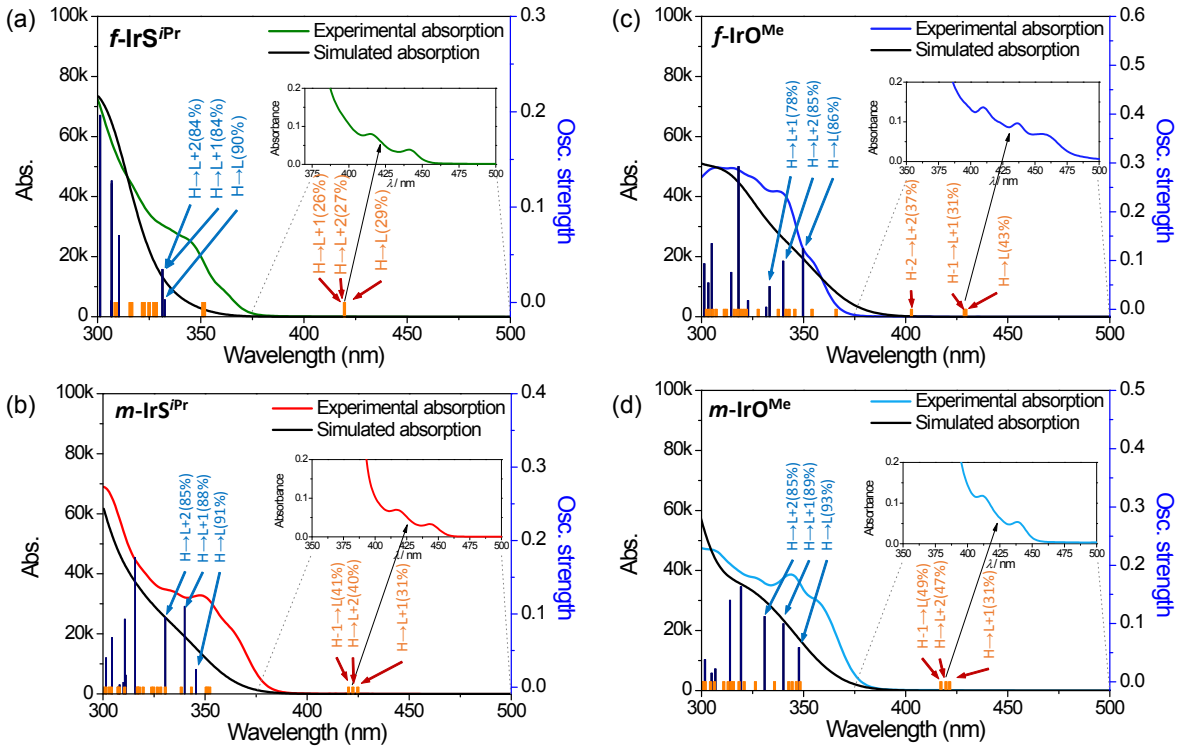

Fig. S10 Experimental and calculated absorption spectra and singlet transition for Ir complexes.

Table S7 Calculated transition energy and orbital transition analysis of Ir complexes

	State	λ_{cal} (E_{cal})	*f*	Orbital Contributions	Assignment
***f*-IrS^{iPr}**	T_1	420 nm (2.95 eV)	-	H→L (29%), H-1→L+2 (13%)	MLCT, ILCT
	S_1	332 nm (3.73 eV)	0.003	H→L (90%)	MLCT, ILCT
	S_2	331 nm (3.75 eV)	0.034	H→L+1 (84%)	MLCT, LLCT, ILCT
	S_3	331 nm (3.75 eV)	0.034	H→L+2 (84%)	MLCT, LLCT, ILCT
***m*-IrS^{iPr}**	T_1	425 nm (2.92 eV)	-	H→L+1 (31%), H-1→L+1 (12%)	MLCT, LLCT
	S_1	346 nm (3.58 eV)	0.024	H→L (91%)	MLCT, LLCT
	S_2	340 nm (3.65 eV)	0.110	H→L+1 (88%)	MLCT, LLCT
	S_3	330 nm (3.76 eV)	0.095	H→L+2 (85%)	MLCT, LLCT, ILCT
***f*-IrO^{Me}**	T_1	429 nm (2.89 eV)	-	H-1→L+1 (31%), H-1→L (20%)	MLCT, ILCT
	S_1	349 nm (3.55 eV)	0.124	H→L (86%)	MLCT, LLCT
	S_2	339 nm (3.66 eV)	0.099	H→L+2 (85%)	MLCT, LLCT
	S_3	333 nm (3.72 eV)	0.047	H→L+1 (78%)	MLCT, LLCT
***m*-IrO^{Me}**	T_1	421 nm (2.94 eV)	-	H→L+1 (31%), H-2→L+1 (22%)	MLCT, LLCT, ILCT
	S_1	348 nm (3.56 eV)	0.059	H→L (93%)	MLCT, LLCT
	S_2	340 nm (3.65 eV)	0.100	H→L+1 (89%)	MLCT, LLCT, ILCT
	S_3	331 nm (3.75 eV)	0.112	H→L+2 (85%)	MLCT, LLCT, ILCT

Table S8 The frontier molecular orbital contribution on iridium metal (Ir), dibenzothiophene (dbt), dibenzofuran (dbf), and imidazolyl (im) moieties

	MO	*E* (eV)	Contribution (%)		
			Ir	dbt or dbf	Im
***m*-IrS^{Me}**	LUMO	− 0.59	2	89	9
	HOMO	− 4.74	27	59	14
	HSOMO	− 2.00	5	90	5
	LSOMO	− 4.91	25	55	19
***f*-IrS^{iPr}**	LUMO	− 0.49	2	77	21
	HOMO	− 4.78	23	60	17
	HSOMO	− 2.08	3	76	21
	LSOMO	− 4.94	17	67	16
***m*-IrS^{iPr}**	LUMO	− 0.57	3	86	11
	HOMO	− 4.72	39	51	10
	HSOMO	− 1.48	2	80	18
	LSOMO	− 4.89	22	66	12
***f*-IrO^{Me}**	LUMO	− 0.46	3	82	14
	HOMO	− 4.75	31	50	19
	HSOMO	− 2.00	4	83	13
	LSOMO	− 4.92	27	59	14
***m*-IrO^{Me}**	LUMO	− 0.55	3	86	11
	HOMO	− 4.67	39	52	9
	HSOMO	− 2.01	4	76	20
	LSOMO	− 4.87	23	67	10

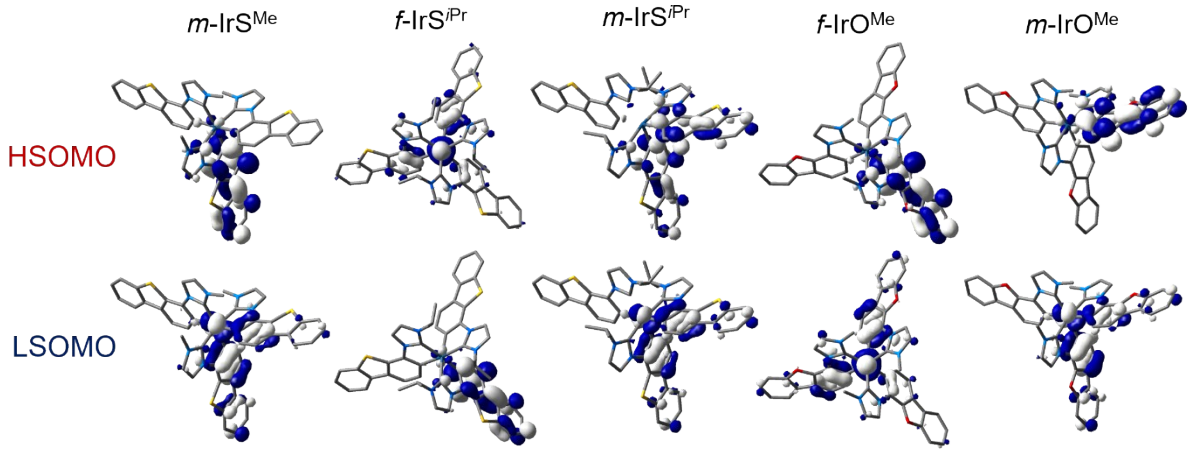

Fig. S11 Frontier molecular orbitals of Ir(III) complexes for triplet manifold.

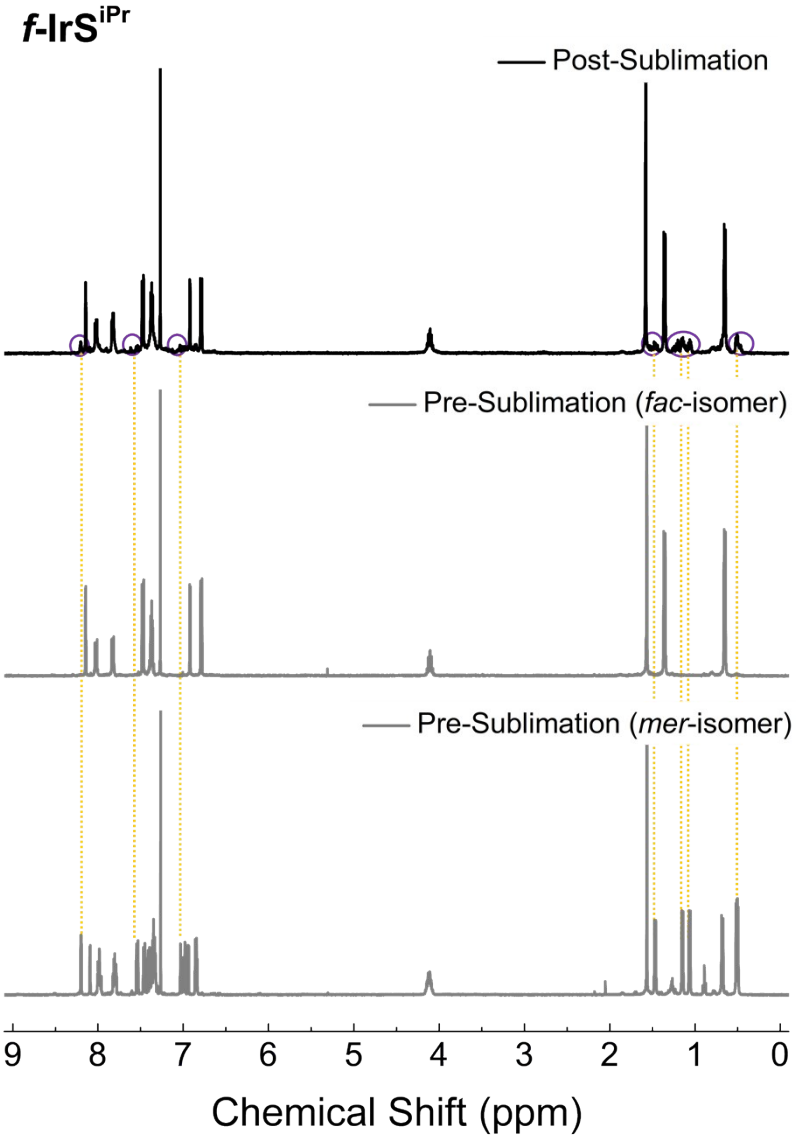

Fig. S12 ^{1}H-NMR spectra of ***f*-IrS^{iPr}** before and after sublimation.

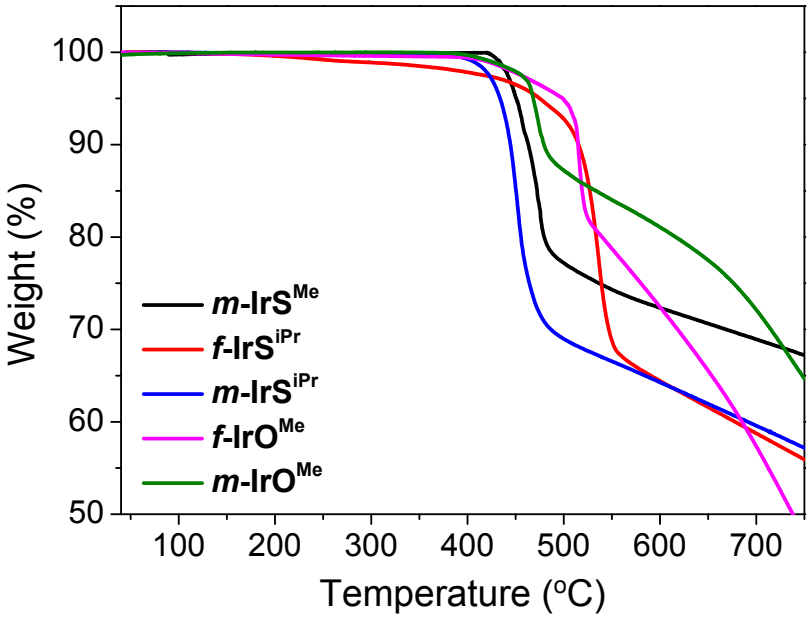

Fig. S13. Thermogravimetric analysis (TGA) curves for Ir(III) complexes. The observed $T_{5\%}$ (temperatures of thermal weight loss 5%) values of more than 400 ℃ indicate that all Ir complexes have high thermal stabilities that are needed for a high-temperature process of device fabrication.

Table S9. TGA thermal parameters for Ir (III) complexes

Complex	Thermal parameters	
	T_d/℃[a]	$T_{5\%}$/℃[b]
***m*-IrS^{Me}**	444	458
***f*-IrS^{iPr}**	511	515
***m*-IrS^{iPr}**	432	435
***f*-IrO^{Me}**	504	507
***m*-IrO^{Me}**	457	459

[a] T_d: onset degradation temperature. [b] $T_{5\%}$: the temperature at 5% weight loss.

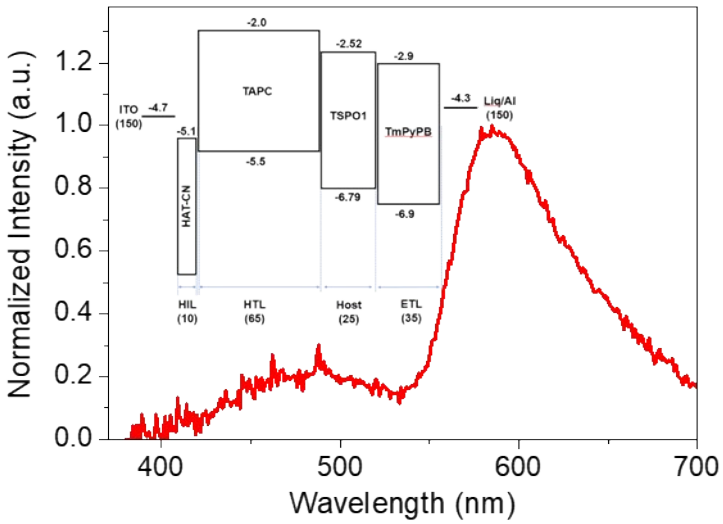

Fig. S14 EL spectra of the TSPO1 (device structure: ITO (150 nm)/HAT-CN (10 nm)/TAPC (65 nm)/TSPO1 (25 nm)/TmPyPB (35nm)/Liq/Al (150nm)). The low intensity of EL spectra in the range 400 to 500 nm reflects that TSPO1 host material has no contribution to the EL emission of the normal device structure with Ir-doped emitting layer (Ir (10%):TSPO1). The peak around 600 nm can be assigned as the emission of electromer, which is originated from electrons injected into TAPC layer, as reported by previous literature.[7-8] Note that the electromer formation on the normal Ir-doped device is effectively suppressed because the exciton formation zone positions mainly in the emitting layer.

References

1. Y.-J. Cho, S. A. Hong, H.-J. Son, W.-S. Han, D. W. Cho and S. O. Kang, *Inorg*. *Chem*., 2014, **53**, 13136.
2. M. J. Frisch, et al., Gaussian 09, Revision D.01, Gaussian Inc., WallingfordCT, 2013.
3. A. D. Becke, *J*. *Chem*. *Phys*., 1993, **98**, 5648.
4. C. Lee, W. Yang and R. G. Parr, *Phys*. *Rev*. *B*: *Condens*. *Matter Mater*. *Phys*., 1988, **37**, 785.
5. SMART and SAINT, Bruker Analytical X-Ray Division, Madison, WI, 2002.
6. G. M. Sheldrick, SHELXTL-PLUS Software Package, Bruker Analytical X-Ray Division, Madison, WI, 2002.
7. J. Kalinowski, G. Giro, M. Cocchi, V. Fattori and P. D. Marco, *Appl. Phys. Lett.*, 2000, **76**, 2352.
8. S. Kwon, K.-R. Wee, C. Pac, and S. O. Kang, *Org*. *Electron*., 2012, **13**, 645.